EUROPEAN ORGANIZATION FOR NUCLEAR RESEARCH

CERN-EP/79-18
7 March 1979

REACTION $\pi^- p \to \pi^0 n$ IN THE 15-40 GeV/c MOMENTUM RANGE

W.D. Apel[1], K.H. Augenstein[1], E. Bertolucci[2], S.V. Donskov[3], A.V. Inyakin[3], R. Johnson[3,4], V.A. Kachanov[3], R.N. Krasnokutsky[3], M. Krüger[1], G. Leder[5], A.A. Lednev[3], I. Mannelli[2,6], Yu.V. Mikhailov[3], H. Müller[1], G.M. Pierazzini[2], Yu.D. Prokoshkin[3], M. Quaglia[2], F. Sergiampietri[2], A. Scribano[2], D. Schinzel[1,6], H. Schneider[1], R.S. Shuvalov[3], G. Sigurdsson[1,6], M. Steuer[5], A.N. Toropin[3] and M.L. Vincelli[2]

Joint experiment of the
Institute for High Energy Physics (Serpukhov, USSR)
and the European Organization for Nuclear Research
(Geneva, Switzerland)

(Submitted to Nuclear Physics B)

1) Institut für Experimentelle Kernphysik, Universität und Kernforschungszentrum, Karlsruhe, Fed. Rep. of Germany.

2) Istituto di Fisica dell'Università, Pisa, and INFN, Sezione di Pisa, Italy.

3) IHEP, Serpukhov, USSR.

4) Visitor from the Lawrence Berkeley Laboratory; now at FNAL, Batavia, USA.

5) Institut für Hochenergiephysik, ÖAdW, Vienna, Austria.

6) Now at CERN, Geneva, Switzerland.

ABSTRACT

A high statistics measurement of the reaction $\pi^- p \to \pi^0 n$ has been performed at the Serpukhov accelerator for 15, 20, 25, 30, and 40 GeV/c incident pion momentum using the NICE set-up with its associated 648-channel hodoscope spectrometer for γ-ray detection. More than 3 million charge-exchange events have been recorded in total.

It is found that the spin-flip and non-spin-flip amplitudes can be parametrized, for small $|t|$, as exponentials with the same slopes to within a few per cent. Also the behaviour of the differential cross-section for small and medium $|t|$ agrees with the prediction of a geometrical s-channel model which describes binary reactions in terms of a complex pole $b_0(s)$. The imaginary part of this universal pole Im $b_0(s)$ has been determined and found to be growing logarithmically with s.

In the present paper we report results on the measurements of the cross-section for the charge-exchange reaction

$$\pi^- p \to \pi^0 n \qquad (1)$$
$$\hookrightarrow 2\gamma$$

carried out with high statistical accuracy and over a wide range of four-momentum transfer t for incident pion momenta p between 15 and 40 GeV/c.

The reaction amplitude for pion charge exchange is known to be dominated at high energies by the contribution in the t channel of the trajectory with the quantum numbers of the ρ meson. The cross-section for reaction (1) has been measured in a number of experiments [1-8] using samples not exceeding a few tens of thousands of events. The results reported below are based on a total of about 3×10^6 recorded π^0. These large statistics have allowed us to extend the useful range of t and to study in detail the behaviour of the cross-section in the region of the forward dip, which reflects the importance of the spin-flip [6] amplitude. Preliminary partial results have been reported previously [9].

The experiment has been performed at the IHEP 70 GeV accelerator using the NICE set-up, described elsewhere [10,11]. The energies and coordinates of the γ-rays from the π^0 decay were measured in a 648-channel hodoscope spectrometer. The pattern recognition and kinematical reconstruction programs are described in ref. 10. The measurements have been carried out at five values of the incident pion momentum (see table 1) for different distances L between the liquid hydrogen target and the γ-ray detector. A number of control measurements [10] have allowed us to evaluate possible systematic errors. In total, during the experiment about 3×10^{11} π^- have gone through the target, corresponding to a sensitivity of about 3×10^{-36} cm^2 per event.

The invariant mass spectrum of γ-ray pairs shows only a very small background in the region of the peak corresponding to the $\pi^0 \to 2\gamma$ from reaction (1) [10]. It is only in the region of large $|t|$, where the cross-section is reduced by 4-5 orders of magnitude with respect to the t = 0 value, that the background reaches values of up to 15%. The main source of background, as described in ref. 10, comes from

wrong identification of a fraction of the large invariant mass π^0 pairs produced in the reaction $\pi^- p \to \pi^0\pi^0 n$.

The values of the integrated cross-section σ measured for reaction (1) are reported in table 2 and shown in fig. 1, together with other results in the momentum range 10-100 GeV/c [2,6,8]. No correction has been applied for electromagnetic effects [12]. The various experiments agree with each other within the limit allowed by the combined statistical and systematic uncertainties: for example at 20.0 GeV/c the difference between the values from refs. 6-8 and our result is (+4 ± 6)% [6], (-3 ± 6)% [7], (+3 ± 6)% [8], and at 40.0 GeV/c (+5 ± 8)% [6], (-10 ± 7)% [7] and (-6 ± 7)% [8].

The energy dependence of the integrated cross-section σ for reaction (1) is well described by

$$\sigma = (122 \pm 8)(s/s_0)^{-1.23\pm0.02} \times 10^{-30} \text{ cm}^2 \qquad (2)$$

(the line in fig. 1), where s is the square of the energy in the $\pi^- p$ centre-of-mass system and $s_0 = 10$ GeV^2. The values above have been obtained by a least squares fit of all our results and those of ref. 8, taking into account systematic errors.

The measured values of the differential cross-section for reaction (1) are given in table 3. The sample with the highest statistics was obtained at 40 GeV/c, where the differential cross-section changes by five orders of magnitude over the $|t|$ range 0-2 (GeV/c)^2. The t-dependence of the differential cross-section is shown in fig. 2 in terms of the values of $d\sigma/\sigma dt$ which are practically free of systematic errors and allow a more meaningful comparison with the results from other experiments. As shown in table 3 and fig. 3, the forward dip of the differential cross-section is clearly seen for all values of the incident π^- momentum and there is no irregularity in shape. The fluctuations previously observed [8] are evidently of a purely statistical nature.

As has been shown in ref. 6, at high energy and small $|t|$, the amplitude for reaction (1) may be parametrized as follows:

$$\begin{aligned} F_+(t) &= f_+(t)\, e^{c_+ t/2} \\ F_-(t) &= \sqrt{-t}\, f_-(t)\, e^{c_- t/2}\ , \end{aligned} \qquad (3)$$

where $F_+(t)$ and $F_-(t)$ are the spin-non-flip and spin-flip amplitudes and $f_\pm(t)$ are slowly varying functions of t. Making the assumption that

$$c_+ = c_- = c \tag{4}$$

and also $f_\pm(t) \simeq$ constant for small $|t|$, the differential cross-section for reaction (1) would take the form

$$\frac{d\sigma}{dt} = \left.\frac{d\sigma}{dt}\right|_{t=0} \times (1 - gct)\, e^{ct} , \tag{5}$$

where g is the ratio of the integrated cross-sections with and without spin flip. In a previous analysis [6] the dependence (5) was found to be adequate for the description of data with $|t| \lesssim 0.4$ $(GeV/c)^2$, but the statistics available were not sufficient to test the assumption (4). This has been possible with the data of the present experiment and indeed the values of c_+ and c_- resulting from the fit coincide within the measuring errors ($\lesssim 3\%$). They also remained practically unchanged when varying the $|t|$ range used in the fit (see table 3). It is remarkable that the same result is true for the reaction $\pi^- p \to \eta n$ [10]. Evidently, this experimental finding can hardly be accidental and demands a corresponding theoretical explanation.

The quality of the description of the data in terms of the expression (5) can be judged from fig. 3. The values of the parameters c and g, resulting from the least squares fit of the data of the present experiment and of other results [2,8] at lower and higher incident momenta (only data with sufficient statistics and adequate t resolutions have been used for the fit), are plotted in fig. 4. It can be seen that with increasing incident momentum p the slope c of the forward peak increases as ln p, while the ratio g of spin-flip to non-spin-flip cross-section decreases slightly. In the range $15 \leq p \leq 40$ GeV/c of the present experiment the spin-flip cross-section is dominant ($g \simeq 2$).

The values of the differential cross-section for reaction (1) at $t = 0$ obtained by extrapolation of the best fit dependence (5) are plotted in fig. 5. Their energy dependence, including the systematic errors of the present experiment and

of ref. 8 used in the fit, is well described by $(s/s_0)^{-1.04\pm0.02}$. The value of the intercept for the effective trajectory is consequently found to be

$$\alpha_\rho(0) = 0.48 \pm 0.01 \ . \tag{6}$$

It is worth while remarking that up to 40 GeV/c the values of $d\sigma/dt|_{t=0}$ for reaction (1) agree well with the predictions from the measured values of the difference between the π^+p and π^-p total cross-sections, based on dispersion relations and charge invariance. At higher energies the FNAL data [8] (see also refs. 14 and 15) are not easily reconciled with the total cross-section measurements [13].

The results shown in figs. 4 and 5 for the $10 \leq p \leq 200$ GeV/c momentum range and small $|t|$ can be summarized by the following phenomenological description

$$\frac{d\sigma}{dt}(s,t) = A\left(\frac{s}{s_0}\right)^{2\alpha_\rho(0)-2} \left[1 - g(s)c(s)t\right] e^{c(s)t} \tag{7}$$

$$c(s) = c_0 + c_1 \ln (s/s_0) \tag{8}$$

$$g(s) = g_0 + g_1 \ln (s/s_0) \tag{9}$$

with

$$\begin{aligned} A &= (435 \pm 20) \times 10^{-30} \text{ cm}^2 \text{ (GeV/c)}^{-2} \\ g_0 &= 2.55 \pm 0.09 \\ g_1 &= -0.23 \pm 0.06 \\ c_0 &= 12.7 \pm 0.3 \text{ (GeV/c)}^{-2} \\ c_1 &= 1.57 \pm 0.12 \text{ (GeV/c)}^{-2} \\ \alpha_\rho(0) &= 0.48 \pm 0.01 \end{aligned} \tag{10}$$

The single Regge-pole exchange model would predict a power-law dependence at fixed t [16]

$$\frac{d\sigma}{dt}(s,t) = B(t)\left(\frac{s}{s_0}\right)^{2\alpha_\rho(t)-2} , \tag{11}$$

which is found empirically to be approximately valid for reaction (1) up to the highest measured incident momenta at small and medium $|t|$. However, as can be seen from fig. 6, where $d\sigma/dt$ is plotted as a function of the incident momentum p for some representative fixed value of t, while at small t the Regge parametrization is indeed quite good, the FNAL data [8] at $p \geq 60$ GeV/c and $|t| \gtrsim 1$ (GeV/c)^2

show a deviation from the Regge behaviour as determined by the data of the present experiment (in the sense of a too slow decrease of the differential cross-section at fixed $|t|$ versus p) which, if not due to undetected background, could represent a breakdown of the Regge picture at high p and $|t|$.

The ρ effective trajectory $\alpha_\rho(t)$, as determined from the data of the present experiment in the range $15 \leq p \leq 40$ GeV/c and $|t|$ up to 2 $(\text{GeV/c})^2$, is shown in fig. 7. The trajectory is approximated by a straight line $\alpha_\rho(t) = 0.48 + 0.90\ t$, which extrapolates to the ρ and g masses at the corresponding spin values. Essentially the same trajectory is found by including in the fit experiments at lower p values, while if the data [8] are used, a strong non-linearity appears for $|t| \gtrsim 1$ $(\text{GeV/c})^2$. As already remarked above, in this p, $|t|$ region the Regge picture itself may indeed not describe the data any more adequately. Clearly, further accurate measurements covering an expanded kinematical range are crucial in order to clarify the situation.

The high statistics of the present experiment and the range of $|t|$ extending well beyond the region of the second maximum (see fig. 8) have allowed useful comparisons of the data with other models, in particular, with the geometric s-channel approach by Schrempp and Schrempp [17] which, using a universal complex pole $b_0(s)$, describes the t dependence of a number of binary reactions ($\pi^- p \to \pi^0 n$, $\pi^- p \to \eta n$, $K^- p \to \bar{K}^0 n$, $\pi^- p \to \Lambda^0 K^0$, etc.) for $|t| \gtrsim 0.25$ $(\text{GeV/c})^2$. For reaction (1) the model predicts that the value of $\ln \sqrt{-t}\ d\sigma/dt$ oscillates with increasing $\sqrt{-t}$ between two parallel straight lines of the following equation

$$\ln \sqrt{-t}\ d\sigma/dt = -2\ \text{Im}\ b_0(s)\ \sqrt{-t} + A_{1,2}(s)\ . \qquad (12)$$

The value of $2\ \text{Im}\ b_0(s)$ can then be determined as the slope of the tangent to the maxima (minima) of $\ln \sqrt{-t}\ d\sigma/dt$ as a function of $\sqrt{-t}$ (fig. 9).

The results are reported in table 4 and plotted in fig. 10, together with values obtained at lower energies [3,18]. The experiments at higher energies [8] do not cover the necessary $|t|$ range. Clearly, up to $s \simeq 80$ GeV^2, $\text{Im}\ b_0(s)$ is a linear function of $\ln s$. The $\text{Re}\ b_0(s)$ can also be calculated [17] and is found to be $\simeq 5$ $(\text{GeV/c})^{-1}$, corresponding to an interaction radius of about 1 fermi.

The authors wish to thank the Directorates of IHEP and CERN for their support of the NICE experiment. The participants from Karlsruhe also express their thanks to the Bundesministerium für Forschung und Technologie for financial support.

REFERENCES

[1] I. Mannelli et al., Phys. Rev. Lett. 14 (1965) 408.

[2] A.V. Stirling et al., Phys. Rev. Lett. 14 (1965) 763.

[3] P. Sonderegger et al., Phys. Lett. 20 (1965) 75.

[4] M.A. Wahlig and I. Mannelli, Phys. Rev. 168 (1968) 1515.

[5] V.N. Bolotov et al., Preprint IHEP 71-95, Serpukhov, 1971; Phys. Lett. 38B (1972) 120.

[6] V.N. Bolotov et al., Preprint IHEP 73-52, Serpukhov, 1973; Yadernaya Fiz. 18 (1973) 1046; Nucl. Phys. 37B (1974) 365.

[7] A.V. Barnes et al., Proc. 17th Internat. Conf. on High Energy Physics, London, 1974 (Rutherford Lab., Chilton, Didcot, 1974), p. I-37.

[8] A.V. Barnes et al., Phys. Rev. Lett. 37 (1976) 76.

[9] W.D. Apel et al., JETP Lett. 26 (1977) 659; Phys. Lett. 72B (1977) 132; K.H. Augenstein, Preprint KfK-Ext 3/78-3 Karlsruhe, 1978.

[10] W.D. Apel et al., Preprint IHEP 79-1, Serpukhov, 1979, to be published in Nuclear Physics B.

[11] Yu.V. Bushnin et al., Preprint IHEP 74-21, Serpukhov, 1974; Nucl. Instrum. Methods, 120 (1974) 391.

[12] E. Borie and H.P. Jakob, Phys. Lett. 78B (1978) 323;
I.N. Ginzburg, G.L. Kotkin and V.G. Serbo, Phys. Lett. 80B (1978) 101.

[13] A.S. Carroll et al., Phys. Lett. 61B (1976) 303.

[14] A. Garcia et al., Trieste International Centre, Report IC/77/9 (1977).

[15] H. Nakata, Phys. Rev. D 15 (1977) 927.

[16] R.J.N. Phillips and W. Rarita, Phys. Rev. Lett. 15 (1965) 807.

[17] B. Schrempp and F. Schrempp, Nucl. Phys. B54 (1973) 525; B60 (1973) 110; Preprints CERN TH.2258, 1976; TH.2319, 1977.

[18] G. Giacomelli et al., πN-data compilation, CERN-HERA 69-1 (1969).

Table 1

Data taking conditions

Momentum[a] p [GeV/c]	Distance L [m]	Number of recorded π^0 mesons in reaction (1)	
		Total	Used for determining the differential cross-sections
15.0[b]	3.5, 5	150×10^3	90×10^3
20.2	5, 7	200×10^3	140×10^3
25.0	3, 6, 9	500×10^3	300×10^3
30.0	6, 9	200×10^3	140×10^3
40.0	3, 5, 10, 14	1600×10^3	1200×10^3

a) Momentum spread $\Delta p/p = 0.5\text{-}1.5\%$.

b) To obtain a beam having a momentum of 15 GeV/c, the accelerator was tuned to an energy of $E_0 = 30$ GeV. In the remaining cases $E_0 = 70$ GeV.

Table 2

Integrated cross-sections for reaction (1)

p [GeV/c]	σ a) [10^{-30} cm^2]
15.0	34.2 ± 1.8
20.2	22.8 ± 1.1
25.0	17.8 ± 0.8
30.0	14.3 ± 0.7
40.0	10.6 ± 0.5

a) The errors include also a systematic uncertainty of 4% common to all momenta

Table 3

Differential cross-section $d\sigma/dt$[a] for reaction (1) in 10^{-30} cm^2/(GeV/c)^2

Δt [(GeV/c)^2]	$\bar{t}$ [(GeV/c)^2]	p [GeV/c]				
		15.0	20.2	25.0	30.0	40.0
0–0.004	0.002	151 ± 5	108 ± 3	85.3 ± 2.4	72.9 ± 2.1	57.6 ± 1.6
0.004–0.008	0.006	166 ± 6	113 ± 3	91.1 ± 2.5	75.8 ± 2.3	59.5 ± 1.7
0.008–0.012	0.010	180 ± 6	119 ± 3	96.1 ± 2.6	79.6 ± 2.4	62.3 ± 1.8
0.012–0.016	0.014	184 ± 6	120 ± 4	99.3 ± 2.7	81.9 ± 2.4	63.0 ± 1.8
0.016–0.020	0.018	190 ± 6	123 ± 4	102.9 ± 2.8	85.8 ± 2.5	65.6 ± 1.8
0.020–0.024	0.022	196 ± 6	131 ± 4	105.4 ± 2.8	88.1 ± 2.7	67.0 ± 1.8
0.024–0.028	0.026	198 ± 6	134 ± 4	106.1 ± 2.8	89.5 ± 2.7	66.4 ± 1.8
0.028–0.036	0.032	195 ± 6	135 ± 4	106.3 ± 2.5	89.7 ± 2.5	67.1 ± 1.7
0.036–0.044	0.040	198 ± 6	132 ± 4	107.8 ± 2.5	88.5 ± 2.5	67.5 ± 1.7
0.044–0.052	0.048	192 ± 6	132 ± 4	103.6 ± 2.5	87.4 ± 2.5	65.2 ± 1.7
0.052–0.060	0.056	186 ± 6	130 ± 4	100.4 ± 2.5	84.4 ± 2.4	63.6 ± 1.7
0.060–0.068	0.064	186 ± 6	127 ± 4	97.9 ± 2.5	80.9 ± 2.3	62.0 ± 1.7
0.068–0.076	0.072	180 ± 5	121 ± 4	94.5 ± 2.4	77.4 ± 2.3	59.4 ± 1.6
0.076–0.084	0.080	169 ± 5	116 ± 3	91.3 ± 2.3	73.4 ± 2.1	56.9 ± 1.6
0.084–0.092	0.088	158 ± 5	110 ± 3	87.4 ± 2.2	71.5 ± 2.0	53.0 ± 1.5
0.092–0.100	0.096	155 ± 5	102 ± 3	82.6 ± 2.2	65.8 ± 1.9	50.7 ± 1.5
0.100–0.108	0.104	141 ± 4	98.7 ± 3.0	76.9 ± 2.2	63.8 ± 1.8	45.5 ± 1.4
0.108–0.116	0.112	134 ± 4	93.5 ± 2.7	73.0 ± 2.1	57.3 ± 1.7	43.8 ± 1.3
0.116–0.124	0.120	129 ± 4	85.0 ± 2.5	68.2 ± 2.0	54.1 ± 1.6	39.8 ± 1.2
0.124–0.132	0.128	120 ± 4	82.7 ± 2.5	64.4 ± 2.0	49.9 ± 1.5	38.3 ± 1.2
0.132–0.140	0.136	109 ± 3	75.7 ± 2.3	60.5 ± 1.9	47.6 ± 1.4	34.7 ± 1.0

a) The errors quoted do not include an over-all normalization uncertainty of 4%, which is common to all points.

Table 3 (Cont.)

Δt $[(GeV/c)^2]$	$\bar{t}$ $[(GeV/c)^2]$	p [GeV/c]				
		15.0	20.2	25.0	30.0	40.0
0.14-0.15	0.145	105 ± 3	70.7 ± 2.2	54.8 ± 1.8	43.9 ± 1.3	31.4 ± 1.0
0.15-0.16	0.155	94 ± 3	65.2 ± 2.1	50.0 ± 1.6	38.9 ± 1.2	27.1 ± 0.9
0.16-0.17	0.165	89 ± 3	58.4 ± 2.0	44.7 ± 1.4	35.5 ± 1.1	26.0 ± 0.9
0.17-0.18	0.175	82 ± 3	53.6 ± 1.9	40.6 ± 1.3	31.6 ± 1.0	22.8 ± 0.8
0.18-0.19	0.185	74 ± 2	48.6 ± 1.7	37.0 ± 1.1	28.5 ± 0.9	20.5 ± 0.7
0.19-0.20	0.195	66 ± 2	42.6 ± 1.5	33.8 ± 1.0	24.3 ± 0.8	18.7 ± 0.6
0.20-0.22	0.21	56 ± 2	36.9 ± 1.2	27.9 ± 0.7	22.0 ± 0.7	15.0 ± 0.5
0.22-0.24	0.23	48 ± 2	28.7 ± 1.0	23.0 ± 0.6	17.2 ± 0.6	12.0 ± 0.4
0.24-0.26	0.25	37 ± 1	23.3 ± 0.9	17.6 ± 0.5	13.7 ± 0.4	9.4 ± 0.3
0.26-0.28	0.27	29 ± 1	18.5 ± 0.8	14.0 ± 0.4	10.4 ± 0.3	7.5 ± 0.2
0.28-0.30	0.29	23 ± 1	14.6 ± 0.7	10.9 ± 0.3	8.2 ± 0.2	5.6 ± 0.2
0.30-0.34	0.32	16.0 ± 0.6	10.0 ± 0.4	7.41 ± 0.24	5.46 ± 0.17	3.86 ± 0.12
0.34-0.38	0.36	9.7 ± 0.4	6.0 ± 0.4	4.02 ± 0.13	2.83 ± 0.10	2.02 ± 0.06
0.38-0.42	0.40	5.30 ± 0.28	3.08 ± 0.18	2.38 ± 0.08	1.72 ± 0.06	1.08 ± 0.04
0.42-0.46	0.44	2.91 ± 0.21	1.41 ± 0.14	1.30 ± 0.06	0.83 ± 0.04	0.58 ± 0.03
0.46-0.50	0.48	1.64 ± 0.14	0.82 ± 0.09	0.65 ± 0.04	0.47 ± 0.03	0.31 ± 0.02
0.50-0.54	0.52	0.79 ± 0.11	0.50 ± 0.05	0.41 ± 0.03	0.21 ± 0.04	0.18 ± 0.02
0.54-0.58	0.56	0.58 ± 0.08	0.32 ± 0.05	0.23 ± 0.02	0.17 ± 0.03	0.094 ± 0.014
0.58-0.62	0.60	0.56 ± 0.08	0.27 ± 0.05	0.22 ± 0.02	0.16 ± 0.03	0.122 ± 0.013

Table 3 (Cont.)

Δt $[(GeV/c)^2]$	$\bar{t}$ $[(GeV/c)^2]$	p [GeV/c]				
		15.0	20.2	25.0	30.0	40.0
0.62-0.70	0.66	0.75 ± 0.06	0.44 ± 0.04	0.251 ± 0.018	0.172 ± 0.017	0.110 ± 0.008
0.70-0.78	0.74	1.03 ± 0.08	0.47 ± 0.04	0.324 ± 0.021	0.182 ± 0.018	0.119 ± 0.008
0.78-0.86	0.82	1.05 ± 0.08	0.47 ± 0.04	0.317 ± 0.021	0.207 ± 0.020	0.102 ± 0.008
0.86-0.94	0.90	1.01 ± 0.08	0.49 ± 0.04	0.283 ± 0.018	0.209 ± 0.020	0.092 ± 0.007
0.94-1.02	0.98	0.88 ± 0.07	0.41 ± 0.04	0.228 ± 0.017	0.137 ± 0.017	0.071 ± 0.005
1.02-1.10	1.06	0.70 ± 0.06	0.31 ± 0.04	0.176 ± 0.015	0.112 ± 0.013	0.047 ± 0.005
1.10-1.26	1.18	0.58 ± 0.05	0.21 ± 0.02	0.128 ± 0.009	0.070 ± 0.008	0.031 ± 0.003
1.26-1.42	1.34	0.33 ± 0.05	0.15 ± 0.02	0.075 ± 0.007	0.034 ± 0.006	0.016 ± 0.002
1.42-1.58	1.50	0.181 ± 0.035	0.059 ± 0.012	0.044 ± 0.005	0.016 ± 0.004	0.006 ± 0.001
1.58-1.74	1.66	0.110 ± 0.032	0.036 ± 0.010	0.023 ± 0.005	0.007 ± 0.003	0.0018 ± 0.0005
1.74-2.06	1.90	0.042 ± 0.014	0.021 ± 0.005	0.0064 ± 0.0025	0.0030 ± 0.0015	0.0004 ± 0.0003
2.06-2.38	2.22	0.012 ± 0.008	0.006 ± 0.003	0.0032 ± 0.0015	0.0014 ± 0.0008	-

Table 4

Parametrization of the differential cross-section for reaction (1) at 40 GeV/c

t range for fit $[(GeV/c)^2]$	Best fit to expression (5)			Without condition (4)			
	c $[(GeV/c)^{-2}]$	g	$d\sigma/dt\|_{t=0}$ $[10^{-30}\ cm^2/(GeV/c)^2]$	c_- $[(GeV/c)^{-2}]$	c_+ $[(GeV/c)^{-2}]$	g	$d\sigma/dt\|_{t=0}$ $[10^{-30}\ cm^2/(GeV/c)^2]$
0-0.2	15.9 ± 0.3	2.06 ± 0.09	54.9 ± 1.5	15.9 ± 0.3	15.3 ± 0.4	1.96 ± 0.08	54.9 ± 1.5
0-0.3	15.9 ± 0.2	2.08 ± 0.07	54.7 ± 1.5	15.9 ± 0.2	15.1 ± 0.3	1.92 ± 0.07	54.8 ± 1.5

Table 5

Momentum dependence of Im $b_0(s)$

p [GeV/c]	Im $b_0(s)$ [$(GeV/c)^{-1}$]	Reference
3.07	0.93 ± 0.10	2
3.67	0.83 ± 0.10	"
4.83	1.24 ± 0.12	"
5.9	1.70 ± 0.10	"
13.3	2.60 ± 0.30	"
15.0	3.00 ± 0.10	Present experiment
20.2	3.32 ± 0.10	"
25.0	3.57 ± 0.08	"
30.0	3.85 ± 0.10	"
40.0	4.20 ± 0.10	"

Figure captions

Fig. 1 : Dependence of the cross-section of reaction (1) on the π^- incident momentum p. Notation: ● = data from the present experiment; ∇ = data from refs. 2-4; ○, Δ = data from refs. 6 and 8. The straight line is a power law function (2).

Fig. 2 : Relative differential cross-sections $d\sigma/\sigma dt$ in the region of small $|t|$. Notation: ● = data from the present experiment; ∇, ○, Δ = data from refs. 2, 6, and 8. The curves represent the best fit of expression (5) to our data points. Here and in subsequent drawings the figures on the curves indicate the values of the beam momentum p. The horizontal segments indicate the resolution Δt for some representative values of t.

Fig. 3 : Differential cross-section of reaction (1) for small $|t|$. The curves represent best fits of the expression (5) to our data points.

Fig. 4 : The values of the parameters c and g in formula (5) obtained by fitting the data from the present experiment and from refs. 2 and 8 in the range $0 < |t| < 0.2$ $(GeV/c)^2$. Notation: ● = present experiment; ∇ = ref. 2; Δ = ref. 8. The straight lines represent the logarithmic dependence of eqs. (8) and (9).

Fig. 5 : Differential cross-section for reaction (1) at $t = 0$, obtained by extrapolation according to formula (5). Notation: ● = present experiment; ∇ = ref. 2; Δ = ref. 8. The straight line represents the power law dependence of eq. (7).

Fig. 6 : Dependence on momentum p of the differential cross-section at fixed t. The straight lines represent the dependence (11). Notation: ● = present experiment; ∇ = ref. 2; ○ = ref. 6; Δ = ref. 8. The dashed curves are simply traced through the points of ref. 8.

Fig. 7 : ρ effective trajectory. In the insert the small $|t|$ region is shown in greater detail. Notation: O = present experiment; + = fit obtained using all data in the p range 6-200 GeV/c, taking into account also systematic errors; ● = $\alpha_\rho(0)$ value (6). The dashed curve is the trajectory using only data from ref. 8. The straight line goes through the points corresponding to the ρ and g mesons.

Fig. 8 : Differential cross-section of reaction (1) for p = 15, 25, and 40 GeV/c. The continuous part of the curves represents the expression (7) calculated with the parameters (6) and (10). The dashed curves are simply traced through the data points for $|t| > 0.5$ $(GeV/c)^2$.

Fig. 9 : The quantity $\sqrt{-t}\ d\sigma/dt$ versus $\sqrt{-t}$ for p = 15 and 40 GeV/c. The straight lines are tangent to the maxima (minima) of the curves and their slopes give the imaginary part Im $b_0(s)$ of the universal pole, as defined in ref. 16.

Fig. 10 : Energy dependence of Im $b_0(s)$ [17]. Notation: ● = present experiment; ∇ = data from refs. 2 and 3. The straight line represents the logarithmic dependence (13).

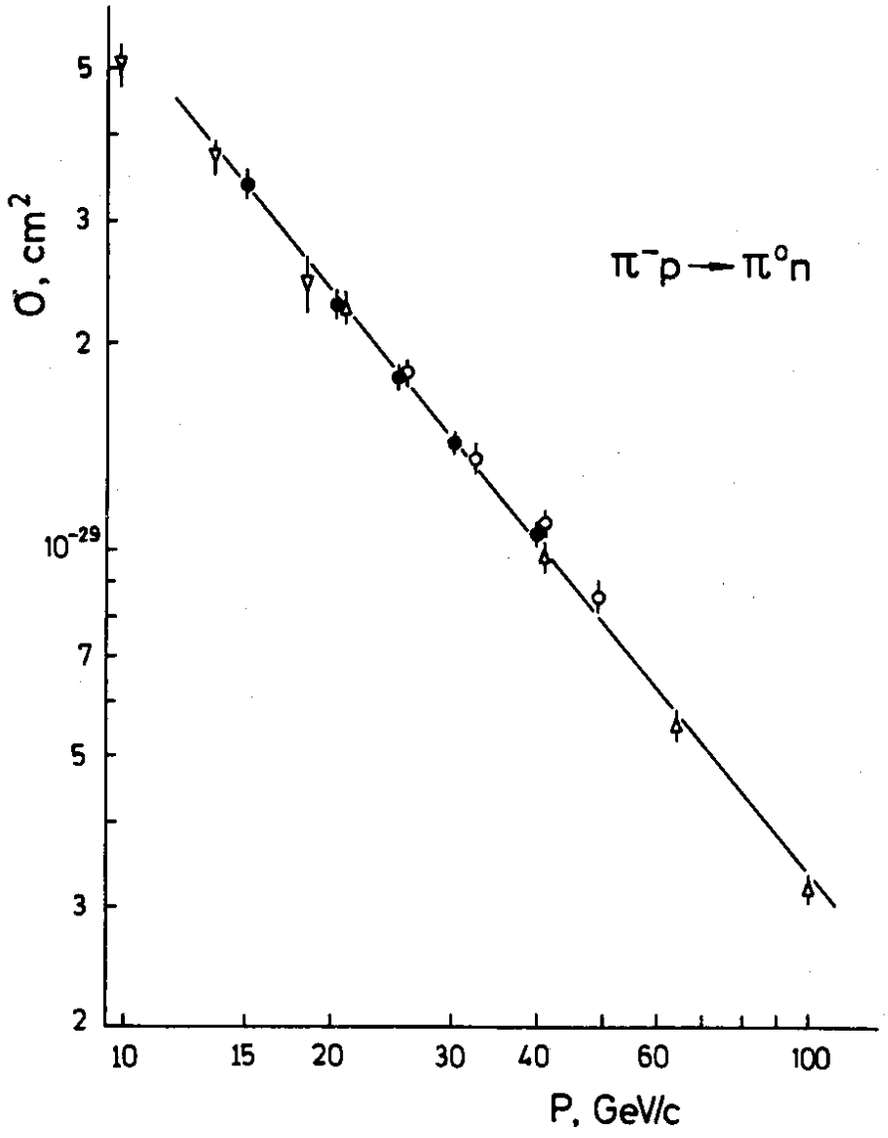

Fig. 1

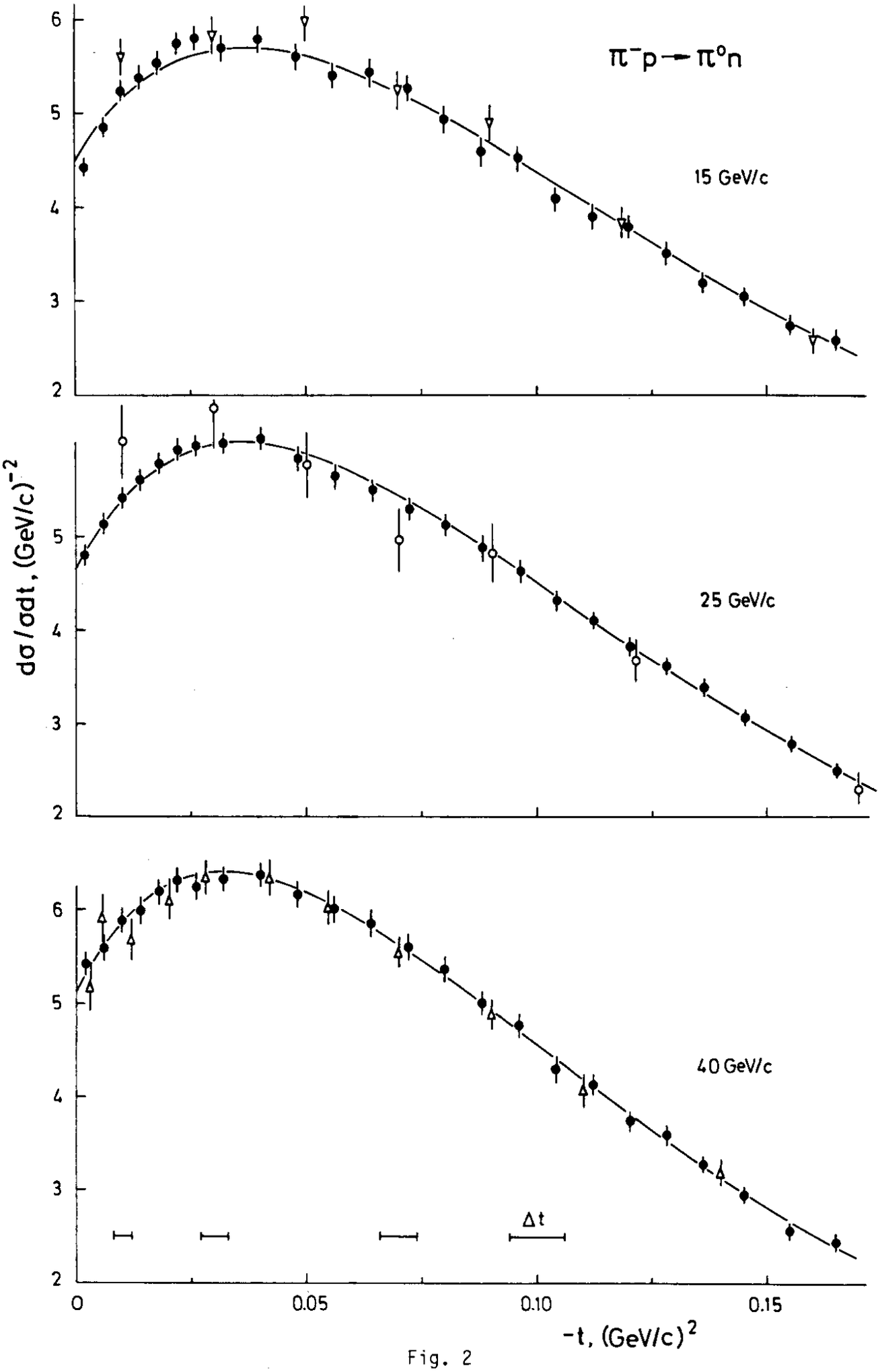
$\pi^- p \to \pi^0 n$
15 GeV/c
25 GeV/c
40 GeV/c
$d\sigma/dt, (GeV/c)^{-2}$
$-t, (GeV/c)^2$
Δt
0
0.05
0.10
0.15
2
3
4
5
6

Fig. 2

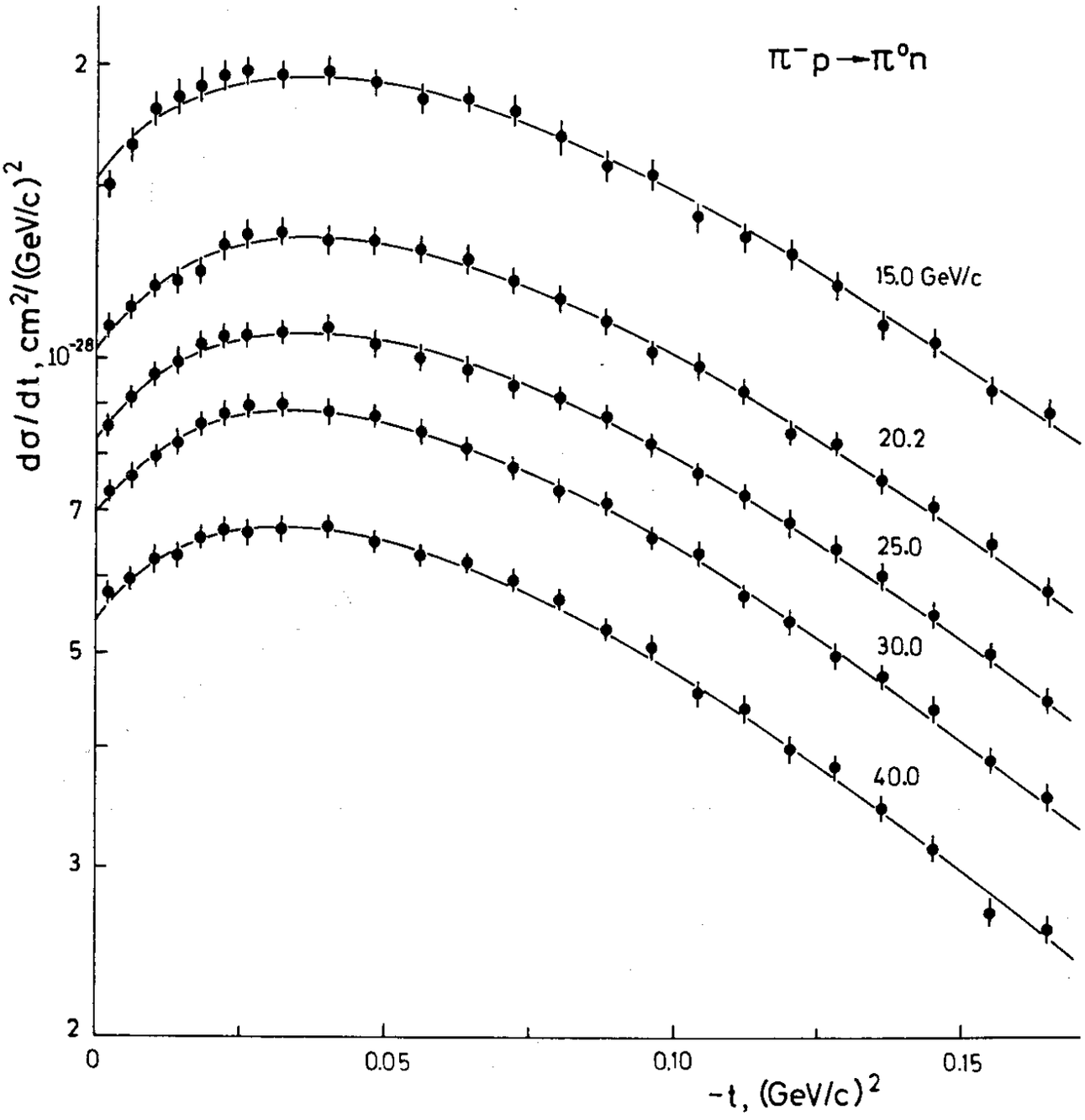
$\pi^- p \to \pi^0 n$
15.0 GeV/c
20.2
25.0
30.0
40.0
$d\sigma/dt$, $cm^2/(GeV/c)^2$
10^{-28}
2
7
5
3
2
0
0.05
0.10
0.15
$-t$, $(GeV/c)^2$

Fig. 3

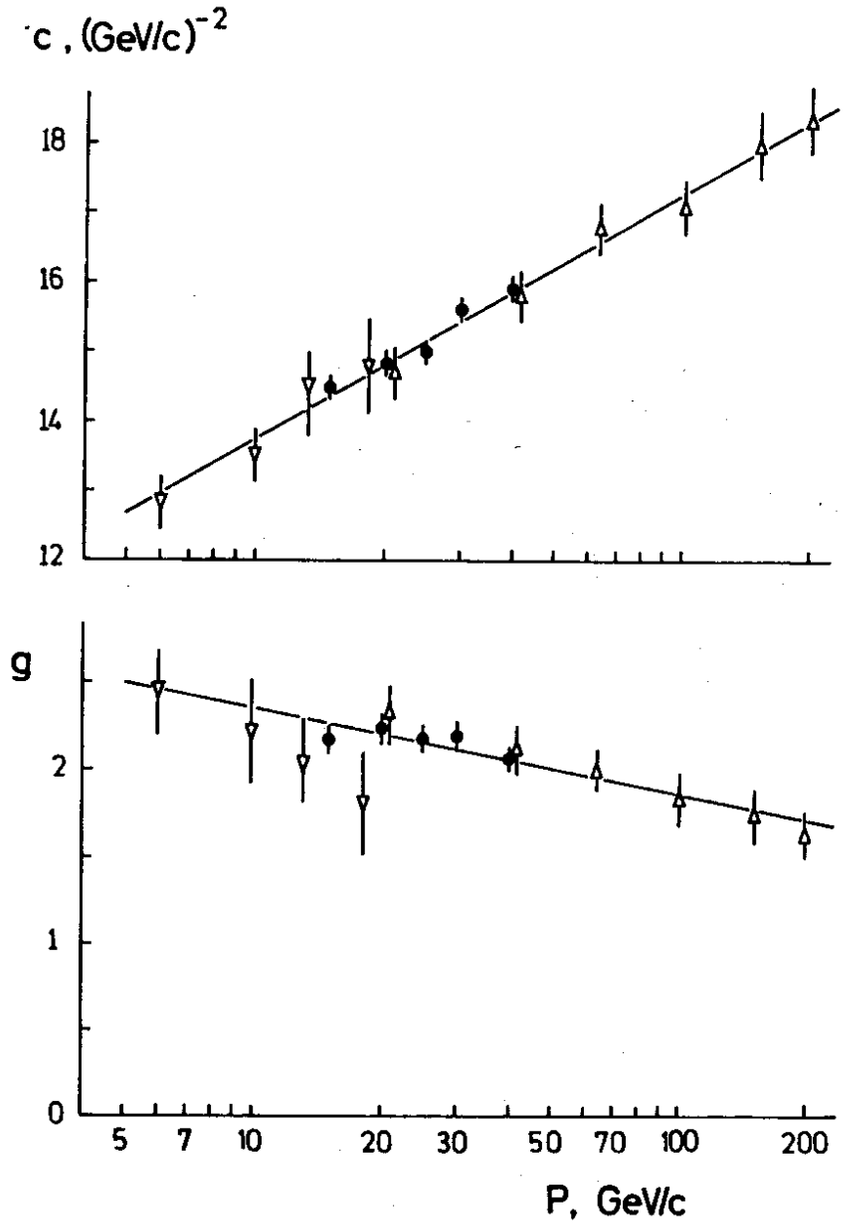
c , (GeV/c)$^{-2}$
18
16
14
12
g
2
1
0
5
7
10
20
30
50
70
100
200
P, GeV/c

Fig. 4

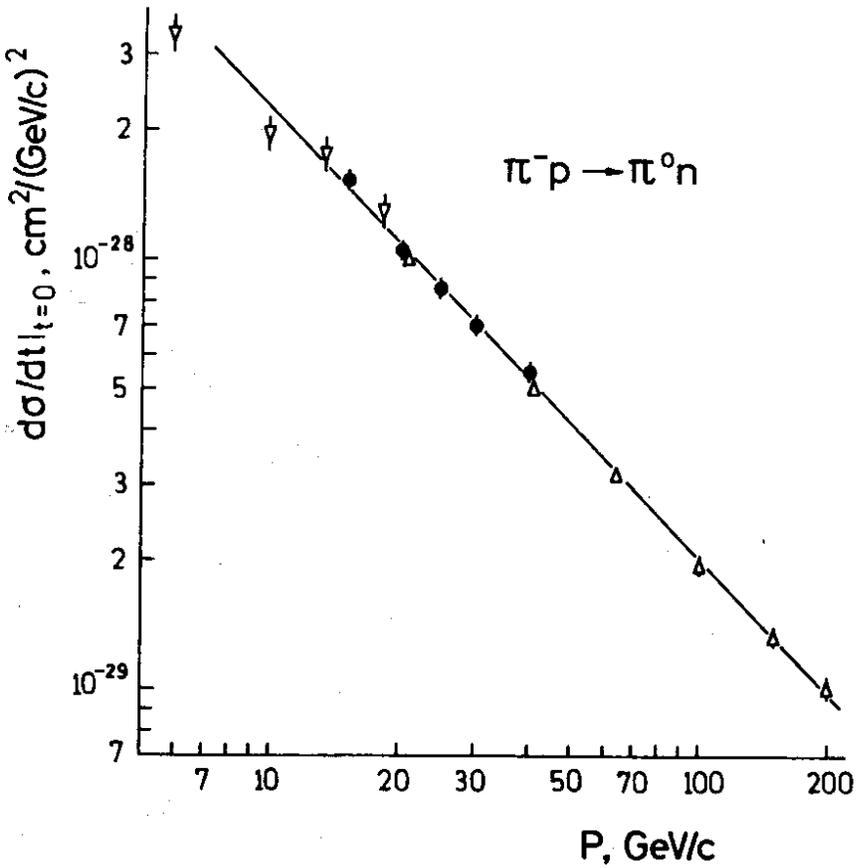
$d\sigma/dt|_{t=0}$, cm^2/(GeV/c)^2
$\pi^- p \rightarrow \pi^0 n$
3
2
10^{-28}
7
5
3
2
10^{-29}
7
7
10
20
30
50
70
100
200
P, GeV/c

Fig. 5

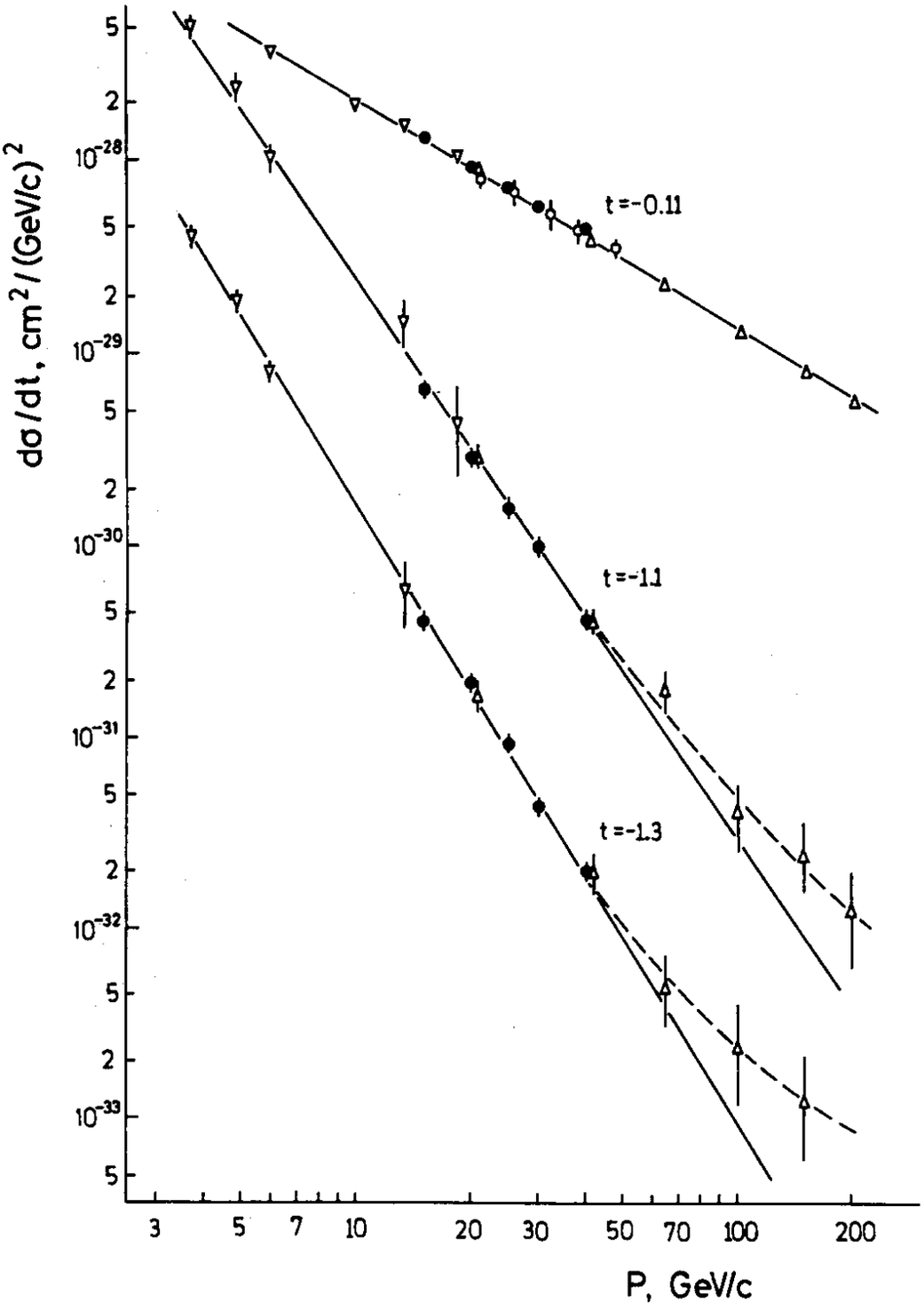

Fig. 6

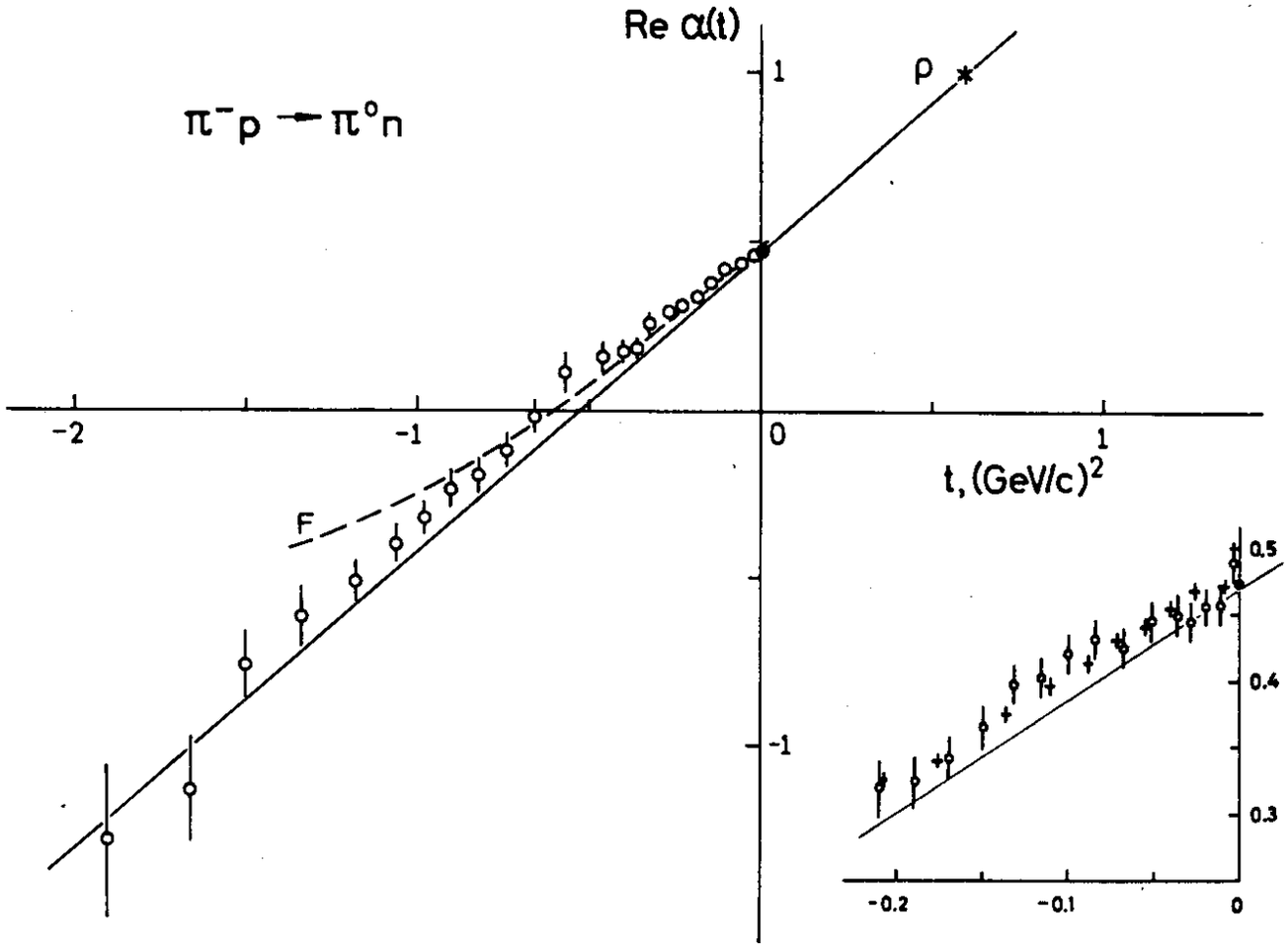

Fig. 7

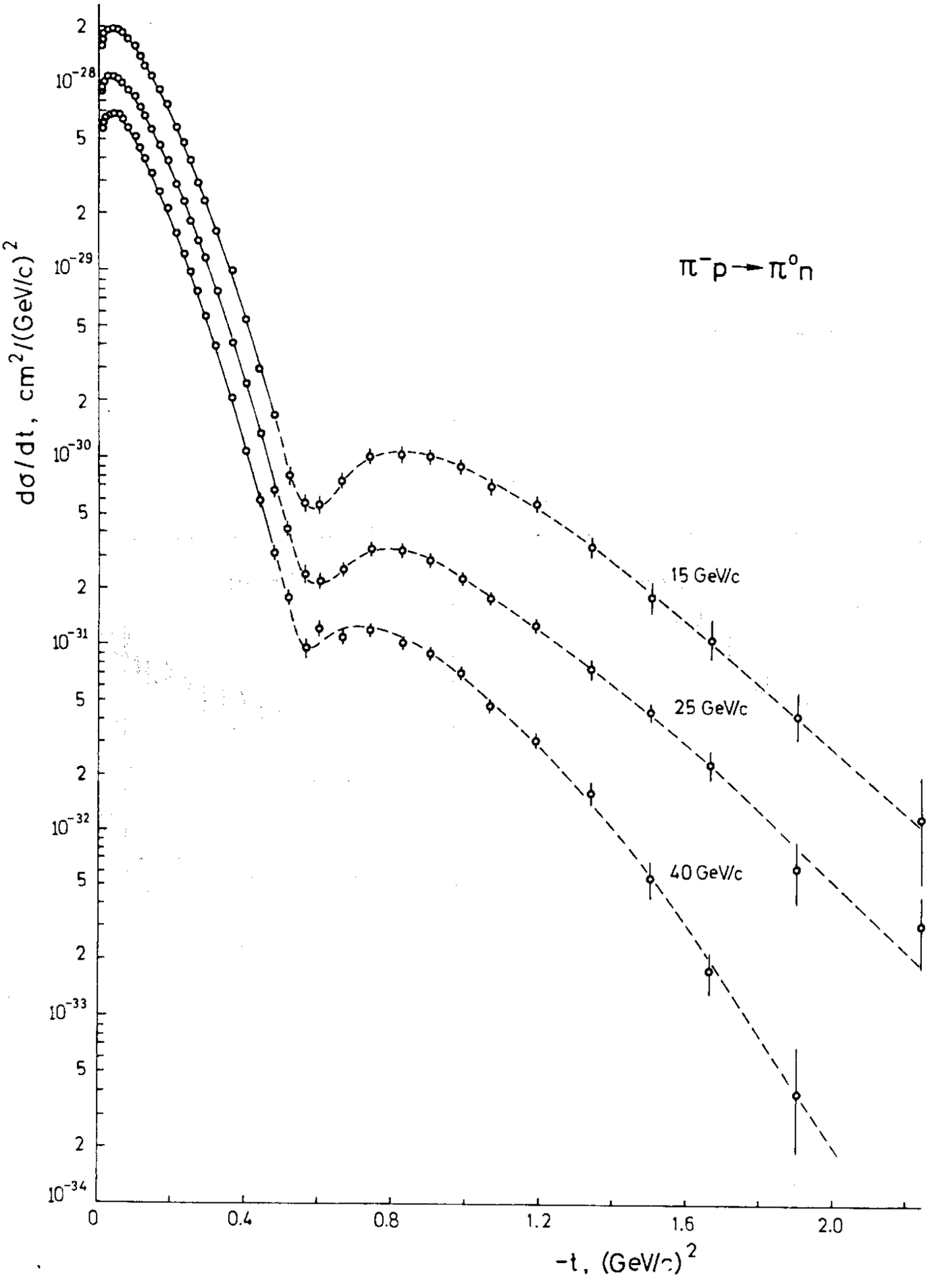
$\pi^- p \rightarrow \pi^0 n$
15 GeV/c
25 GeV/c
40 GeV/c
$d\sigma/dt$, $cm^2/(GeV/c)^2$
$-t$, $(GeV/c)^2$
10^{-28}
10^{-29}
10^{-30}
10^{-31}
10^{-32}
10^{-33}
10^{-34}
0
0.4
0.8
1.2
1.6
2.0

Fig. 8

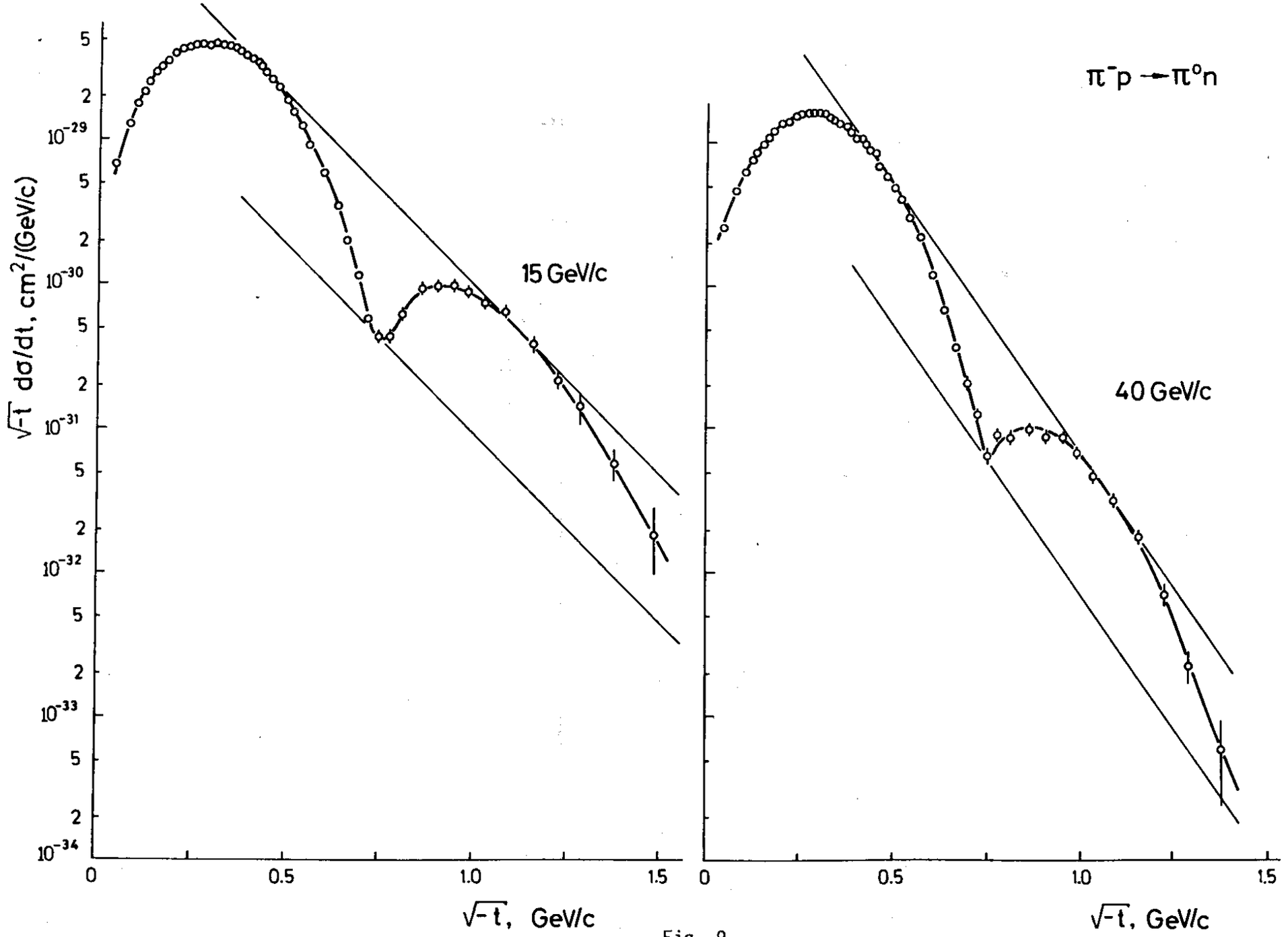
$\pi^- p \to \pi^0 n$
15 GeV/c
40 GeV/c
$\sqrt{-t}\ d\sigma/dt$, $cm^2/(GeV/c)$
$\sqrt{-t}$, GeV/c
$\sqrt{-t}$, GeV/c

Fig. 9

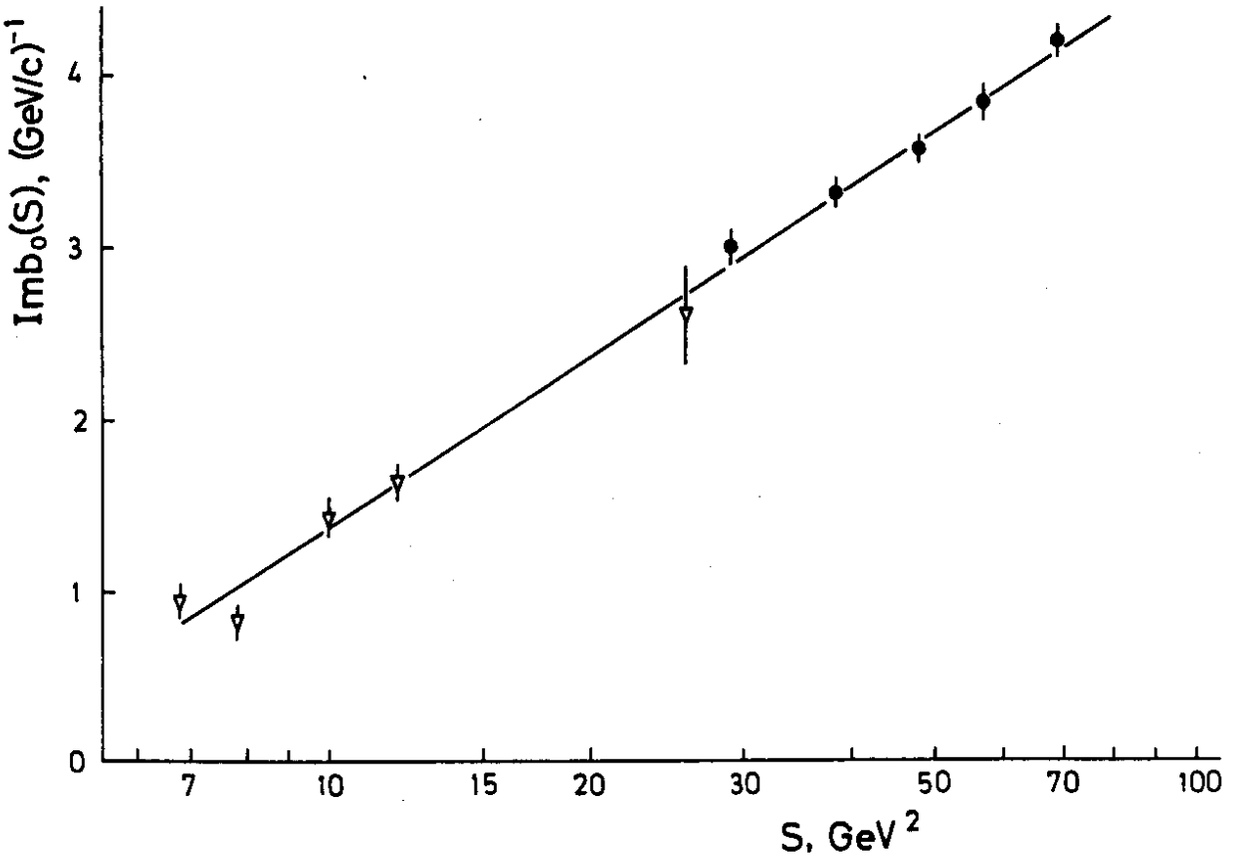

Fig. 10